

Conductance transition with interacting bosons in an Aharonov-Bohm cage

A. R. Kolovsky,^{1,2,3} P. S. Muraev,^{1,2,4} and S. Flach³

¹*Kirensky Institute of Physics, Federal Research Center KSC SB RAS, 660036, Krasnoyarsk, Russia*

²*School of Engineering Physics and Radio Electronics,
Siberian Federal University, 660041, Krasnoyarsk, Russia*

³*Center for Theoretical Physics of Complex Systems,
Institute for Basic Science, 34126 Daejeon, Republic of Korea*

⁴*IRC SQC, Siberian Federal University, 660041, Krasnoyarsk, Russia*

(Dated: July 3, 2023)

We study transport of interacting bosons through an Aharonov-Bohm cage - a building block of flat band networks - with coherent pump and sink leads. In the absence of interactions the cage is insulating due to destructive interference. We find that the cage stays insulating up to a critical value of the pump strength in the presence of mean field interactions, while the quantum regime induces particle pair transport and weak conductance below the critical pump strength. A swift crossover from quantum into the classical regime upon further pump strength increase is observed. We solve the time dependent master equations for the density matrix of the many body problem both in the classical, pure quantum, and pseudoclassical regimes. We start with an empty cage and switch on driving. We characterize the transient dynamics, and the complexity of the resulting steady states and attractors. Our results can be readily realized using experimental platforms involving interacting ultracold atoms and photons on finetuned optical lattices.

Introduction. Flatbands arise in the band structure of finetuned tight-binding networks and are used in various setups in condensed matter physics and photonics [1–4]. Particular interest has been paid to the case when all bands are flat - ABF lattices, as originally observed for particular magnetic flux values threading the lattice, and therefore coined Aharonov-Bohm cages (AB) due to the complete destructive interference induced trapping of noninteracting particles [5, 6]. ABF lattices can be in general diagonalized with a finite number of local unitary transformations, support compact localized eigenstates (CLS), and serve as the starting ground for a variety of single particle and many-body perturbations which lead to different nonperturbative phases of matter [7–18].

A famous example of such an ABF lattice is the π -flux rhombic lattice [6] (also known as the diamond lattice) which is shown in Fig. 1. Here the term " π -flux" means that the sum of phases of the nearest-neighbour hopping matrix elements equals to π . All eigenstates of the quantum particle in this lattice are compact localized states which prohibit any transport across the lattice. This statement, however, is valid only for non-interacting particles. Finite inter-particle interaction will recover transport in general [6, 13, 19], though additional single particle and interaction finetuning can prohibit transport even in the interacting case [11–13, 20].

In the present work we address the effect of inter-particle interaction on the transport of Bose particles across the diamond lattice from the viewpoint of laboratory experiments where one injects bosons into the first site of the lattice by using an external coherent driving pump and withdraws them from the last site with a sink. Nowadays such experiments can be performed by using different physical platforms, for example, superconducting circuits [21–23]. In short, one arranges interacting transmons (micro-resonators coupled to Josephson

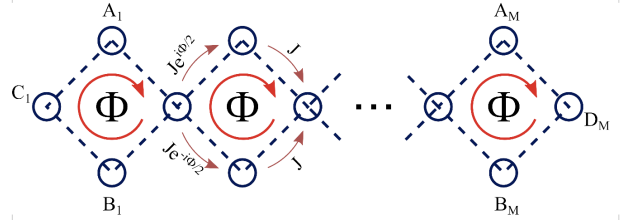


FIG. 1. The flux rhombic lattice (diamond chain). The all bands flat case corresponds to $\Phi = \pi$.

junctions) in a lattice, drives the first transmon with a microwave field, and reads the signal off from the last transmon. The crucial impact of Josephson junctions is that they introduce an effective inter-particle interaction for photons in the micro-resonators. Hence, that setup can be modeled by the Bose-Hubbard Hamiltonian. Another promising system are photonic crystals [24]. In a recent laboratory experiment [25] the authors realized the π -flux rhombic lattice and proved the absence of transport for non-interacting photons.

Model. The above considered laboratory setup is described by the following master equation for the reduced density matrix $\widehat{\mathcal{R}}(t)$ of microwave photons,

$$\frac{\partial \widehat{\mathcal{R}}}{\partial t} = -\frac{i}{\hbar} [\widehat{\mathcal{H}}, \widehat{\mathcal{R}}] - \frac{\gamma}{2} \left(\hat{a}_L^\dagger \hat{a}_L \widehat{\mathcal{R}} - 2\hat{a}_L \widehat{\mathcal{R}} \hat{a}_L^\dagger + \widehat{\mathcal{R}} \hat{a}_L^\dagger \hat{a}_L \right), \quad (1)$$

where γ is the rate of photon absorption by a measure-

ment device and the Hamiltonian $\hat{\mathcal{H}}$ has the form

$$\hat{\mathcal{H}} = \hbar\Delta \sum_{\ell=1}^L \hat{n}_{\ell} - \sum_{\ell,\ell'=1}^L \frac{\hbar J_{\ell,\ell'}}{2} (\hat{a}_{\ell}^{\dagger} \hat{a}_{\ell'} + \text{h.c.}) \quad (2)$$

$$+ \frac{\hbar^2 g}{2} \sum_{\ell=1}^L \hat{n}_{\ell} (\hat{n}_{\ell} - 1) + \frac{\sqrt{\hbar}\Omega}{2} (\hat{a}_1^{\dagger} + \hat{a}_1).$$

In Eqs. (1)-(2) \hat{a}_{ℓ} and \hat{a}_{ℓ}^{\dagger} are the standard annihilation and creation operators which commute to unity, $\hat{n}_{\ell} = \hat{a}_{\ell}^{\dagger} \hat{a}_{\ell}$ is the particle number operator, Ω is the Rabi frequency (which is proportional to the amplitude of the driving field), Δ the detuning of the driving frequency from the linear frequency of quantum oscillators, g the macroscopic interaction constant (which determines the nonlinearity $U = \hbar g$ of the energy spectrum of quantum oscillators), $J_{\ell,\ell'}$ are the hopping matrix elements (i.e., the couplings between oscillators), L is the total number of sites, and \hbar is the dimensionless Planck constant [26]. We label the rhomb sites as shown in Fig. 1 where $C_2 \equiv D_1$, $C_3 \equiv D_2$, etc., and we shall use the gauge where $J_{AD} = J_{BD} = J$ and $J_{CA} = -J_{CB} = iJ$. In what follows we set $J = 1$ which implies that all system parameters are measured in units of the hopping frequency J , and time in units of its inverse $1/J$. The case of non-interacting particles results in destructive interference on the first D -site of the diamond lattice, which blocks all transport. Thus, to understand the effect of finite inter-particle interactions it suffices to consider the lattice consisting of a single rhomb.

Mean field approach. First we analyze the classical (mean-field) problem by using the Gross-Pitaevskii equations on the rhomb lattice, i.e. by replacing annihilation and creation operators by c-numbers in the presence of damping and driving[27]. For the lattice consisting of a single rhomb we have

$$i\dot{C} = (\Delta + g|C|^2) C - \frac{i}{2}A + \frac{i}{2}B + \frac{\Omega}{2} \quad (3)$$

$$i\dot{A} = (\Delta + g|A|^2) A + \frac{i}{2}C - \frac{1}{2}D$$

$$i\dot{B} = (\Delta + g|B|^2) B - \frac{i}{2}C - \frac{1}{2}D$$

$$i\dot{D} = (\Delta + g|D|^2) D - \frac{1}{2}A - \frac{1}{2}B - i\frac{\gamma}{2}D,$$

where C, A, B, D are now time-dependent complex amplitudes of the local oscillators at the rhomb nodes and $\dot{X} \equiv dX/dt$. We use the Rabi frequency Ω as our control parameter and fix $g = 0.5$, $\gamma = 0.2$ and $\Delta = -0.5$. The above equations are invariant under a reflection symmetry $A \rightarrow -B$, $B \rightarrow -A$, with $D = 0$. To enforce $D = 0$ we need $A(t) = -B(t)$. Such states are the generalization of a flatband CLS which persist due to the destructive interference of waves from A and B reaching site D [20].

Due to the presence of dissipation (more precisely, contraction of the phase space volume), the long-time dynamics of system (3) is determined by attractors. At-

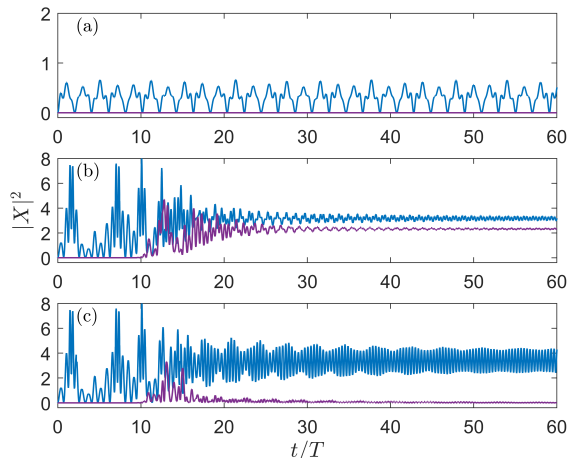


FIG. 2. Relaxation of (3) to various attractors with initial condition $|X| \equiv |A| = |B| = |C| = |D| = 0.001$ and random initial phases. The plots show $|C(t)|^2$ (blue, top line) and $|D(t)|^2$ (purple, bottom line). (a) Relaxation to the symmetric nonstationary attractor s1 for $\Omega = 0.85$. (b) Relaxation to the asymmetric stationary attractor a1 for $\Omega = 1.5$. (c) Relaxation to the symmetric nonstationary attractor s2 for $\Omega = 1.5$ with a tiny change in the initial phase values as compared to case (b). For both (b) and (c) the amplitude $D(t)$ grows exponentially in the interval $0 < t < 10$, all amplitudes show chaotic dynamics during $10 < t < 20$, and the asymptotic regime is obtained for $t \gg 20$. Parameters are $\Delta = -0.5$, $g = 0.5$, $\gamma = 0.2$.

tractors can be stationary (lhs of (3) vanishes) or non-stationary. Stationary attractors can be obtained from Eq. (3) by setting its left-hand-side to zero and solving the remaining nonlinear algebraic equations for the amplitudes A, B, C, D . In addition attractors can be symmetric (they respect the above reflection symmetry) or asymmetric. Asymmetric attractors have $D(t \rightarrow \infty) \neq 0$ and can well be stationary. The current $\bar{j} = \gamma|D|^2$ across the rhomb is nonzero for asymmetric attractors. Symmetric attractors correspond to $D(t \rightarrow \infty) = 0$ and can not be stationary. The current $\bar{j} = \gamma|D|^2$ across the rhomb vanishes for symmetric attractors. The time evolution of $C(t)$, $A(t)$, and $B(t) = -A(t)$ amplitudes of symmetric attractors turns periodic or even quasi-periodic [28]. For $\Omega < \Omega_{cr} \approx 0.9$ we found two symmetric attractors s1 and s2, with s1 smoothly tuned into an empty state $A = B = C = 0$ for $\Omega \rightarrow 0$ and s2 keeping finite constant amplitudes A, B, C in that limit. The attractor s1 turns unstable for $\Omega > \Omega_{cr}$, while attractor s2 stays stable. An asymmetric stationary conducting attractor a1 exists for $\Omega > \Omega_{cr}$.

Conductance Transition. Let us analyze the transport across the rhomb as the function of the Rabi frequency Ω . For small Ω the steady-state response of the system to the external driving is the attractor s1 featuring small quasi-periodic oscillations with $B(t) = -A(t)$ and $D(t) = 0$ (see Fig.2(a)). However, if we increase Ω above

the critical value Ω_{cr} this quasi-periodic trajectory becomes unstable and any tiny perturbation (the numerical round-error suffices) leads to an exponential growth of the D -amplitude. The regime of exponential instability is followed by some transient regime of chaotic dynamics, where all amplitudes show irregular oscillations, see Fig. 2(b,c). The transient chaotic regime is then relaxing into a steady-state regime a1 (Fig.2(b)) or s2 (Fig.2(c)). The exact attractor choice depends on the fine details of the transient state and is again affected by tiny details. Using an ensemble of initial conditions with the absolute values of the complex amplitudes equal to 0.001 and random phases, we calculate the mean values of the squared amplitudes and plot them in Fig. 3(a). One clearly identifies the critical driving magnitude $\Omega_{cr} \approx 0.9$ and this value coincides with the transition from regular to chaotic dynamics in the Hamiltonian counterpart ($\gamma = 0$) of the considered system. Let us also mention that from the viewpoint of a laboratory experiment the crossing of the chaos border is similar to some phase transition where the system is conducting for $\Omega > \Omega_{cr}$ and insulating for $\Omega < \Omega_{cr}$.

Quantum. We proceed with the quantum dynamics. In the numerical simulations we evolve the density matrix $\hat{\mathcal{R}}(t)$ for initial conditions corresponding to the empty system and calculate the single particle density matrix $\hat{\rho}(t)$

$$\rho_{\ell,m}(t) = \text{Tr}[\hat{a}_{\ell}^{\dagger} \hat{a}_m \hat{\mathcal{R}}(t)]. \quad (4)$$

The diagonal elements of this matrix give the population of the rhomb sites while the off-diagonal elements determine the current between the rhomb sites. We also mention the density matrix symmetries $\rho_{A,A}(t) = \rho_{B,B}(t)$, $\rho_{C,B} = -\rho_{C,A}$, and $\rho_{A,B} < 0$, which follow from the π -flux symmetry of the quantum Hamiltonian. Evolving the system for long enough time, we find the stationary population of the rhomb sites, see Fig. 3(c). Note the reasonable agreement between the quantum and classical results for $\Omega > \Omega_{cr}$ and the strong discrepancy for a small Ω . Unlike the classical system, the quantum system remains conducting for $\Omega < \Omega_{cr}$.

To explain the absence of a sharp conductance transition at a critical Ω_{cr} in the quantum case we will consider the system dynamics in Fock space. Let us consider for the moment $\gamma = 0$ and $\Omega = 0$, and an initial state of the system with a non-zero population of the C -site only. The Hamiltonian dynamics will propagate this state into other Fock states. Fig. 4 shows the transition diagram for two particles $N = 2$ where different arrows mean different matrix elements J . For the noninteracting case $g = 0$ the π -flux symmetry of the Hamiltonian induces destructive interference for the Fock states with non-zero occupation of the D -site, preventing our initial Fock state from leaking particles into the D -site. This holds true for larger N as well [29]. Nonzero interactions $g \neq 0$ will detune and remove the destructive interference conditions. In the considered case $N = 2$ these interactions change the equation of motion for the occupation amplitudes of the

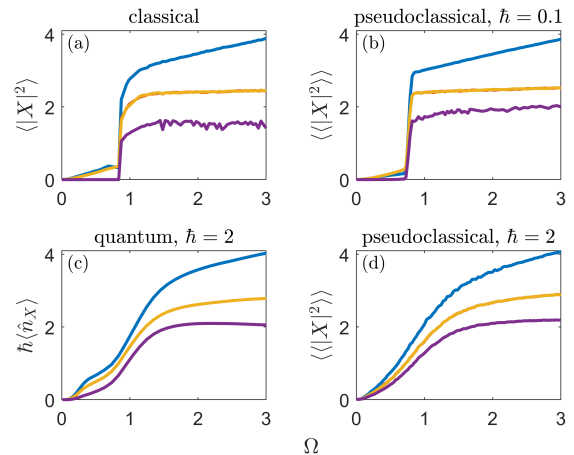


FIG. 3. Left column: (a) The mean squared amplitudes of the classical oscillators in the stationary regime versus Ω , averaged over 1008 random initial phase conditions with $|X| = 0.001$. (c) The mean populations of the rhomb sites for $\hbar = 2$ in the quantum case versus Ω . Right column: The mean squared population of the rhomb sites for the pseudoclassical approach, (b) $\hbar = 0.1$ and (d) $\hbar = 2$. For all cases $|C|^2$ - blue curves (top), $|A|^2$ and $|B|^2$ - yellow curves (middle), $|D|^2$ - purple curves (bottom). The other parameters are $\Delta = -0.5$, $g = 0.5$, and $\gamma = 0.2$. The number of different realizations of the stochastic force in the pseudoclassical approach is 1008.

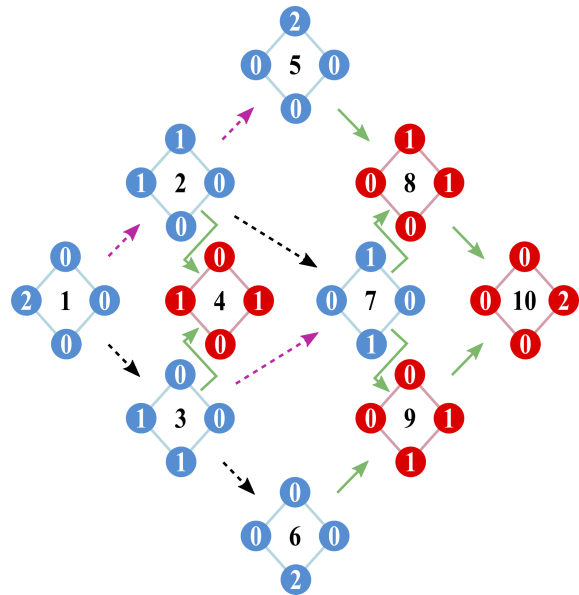


FIG. 4. Transition diagram for two particles $N = 2$. The rhombs present the ten different Fock states which are labeled by the index $j = 1, \dots, 10$ in the center of each rhomb. The numbers of particles on the individual sites of a rhomb in a given Fock state are indicated in the blue and red circles. The dashed red and black arrows correspond to matrix elements $J = \pm i$ and the green arrows to $J = 1$. If $g = 0$ the red-colored Fock states cannot be populated because of complete destructive interference between different paths connecting these states with the initial state $j = 1$.

5th and the 6th Fock states, which leads to a population of the symmetry protected Fock states. We mention, in passing, that for $N = 2$ the discussed interaction-induced destruction of Aharonov-Born caging was confirmed experimentally in the recent experiment [23] with superconducting circuits.

Pseudoclassical. The above presented results prove the quantum system to be always conducting as soon as $g \neq 0$. Thus, the insulator-to-conductor phase transition is a particular feature of the classical system. However, since the transition from the quantum to classical realms is continuous in \hbar , one can find a signature of this classical phase transition in the quantum dynamics if $\hbar \ll 1$. To quantitatively address this problem we resort to the pseudo-classical approximation. The pseudo-classical approximation substitutes the master equation for the reduced density matrix by the Fokker-Planck equation for the classical distribution function $f = f(\mathbf{a}, \mathbf{a}^*, t)$ where a_ℓ and a_ℓ^* are the pairs of canonically conjugated variables ($\ell = 1, \dots, L$),

$$\frac{\partial f}{\partial t} = \{H, f\} + \frac{\gamma}{2} \left(\frac{\partial(a_L f)}{\partial a_L} + \text{h.c.} \right) + \frac{\gamma \hbar}{2} \frac{\partial^2 f}{\partial a_L \partial a_L^*}, \quad (5)$$

where $\{\dots, \dots\}$ denotes the Poisson brackets and H is the classical counterpart of the Bose-Hubbard Hamiltonian (2). The first term in the right-hand-side of this equation corresponds to the Hamiltonian evolution of the system, the next term describes the contraction of the phase space volume, and the last term is the quantum correction to the classical Fokker-Planck equation [30]. This diffusion term is of special importance because it restricts contributions of the other quantum corrections to a value of the order of \hbar^2 [31]. Unfolding the Fokker-Planck equation (5) into the Langevin equation, one arrives to Eq. (3) with an additional stochastic term $\sqrt{\hbar\gamma/2}\xi(t)$. Here $\xi(t)$ is the δ -correlated complex white noise. Then the elements of the single-particle density matrix are found by averaging the solution of the Langevin equation over different realizations of $\xi(t)$, for example, $\rho_{A,B}(t) = \langle A^*(t)B(t) \rangle$. The results of the pseudoclassical approach are shown in the right column in Fig. 3. It is seen that this approach fairly reproduces the exact quantum result for $\hbar = 2$ and indicates the convergence toward the classical result for smaller \hbar .

Conclusion. To summarize, we analyzed the transport of interacting Bose particles across the rhombic lattice (diamond chain) by employing the classical (mean-field), pseudoclassical, and quantum approaches. Within the classical approach the considered problem reduces to the dynamics of coupled nonlinear oscillators, where the first

oscillator in the lattice is driven by an external field and the last oscillator is subject to friction. Then the system is insulating if the stationary amplitude of the last oscillator is strictly zero and conducting if it is finite. Using the driving strength Ω as the control parameter we found the system to be insulating up to a critical Ω_{cr} . When exceeding this critical value, the system becomes unstable, and the transient dynamics of the coupled oscillators turns chaotic. The final state of the system is either conducting or insulating with probability P and $1 - P$, respectively. We found that the discussed probability crucially depends on the system parameters, in particular, on the dissipation constant γ . In brief, for fixed $\Omega > \Omega_{cr}$ this probability monotonically decreases from unity to zero in the interval $0 < \gamma < 0.6$. Thus there is no conducting state for $\gamma > 0.6$ (at least, in the considered interval of Ω). We also studied the many-rhomb system where, to be closer to laboratory experiments, we included small dissipation $\tilde{\gamma} = 0.01$ to all system sites. Importantly, the classification of attractors into symmetric (insulating) and asymmetric (conducting) remains valid. However, for $M > 1$ one finds a zoo of possible attractor combinations. For example, for $M = 3$ there are situations where the first and second rhombs relax to asymmetric attractors but the third rhomb to the symmetric attractor. Yet, the common feature with the single-rhomb system is that the classical limit shows a sharp transition from an insulating to a conducting state at some Ω_{cr} .

Within the quantum approach we numerically solved the master equation for the density matrix of interacting bosons. We found the stationary populations of the lattice sites as a function of the Rabi frequency Ω and compared them with the classical prediction. While there is qualitative agreement with the classical results, one striking difference is that the quantum system conducts even below the threshold $\Omega < \Omega_{cr}$, and the sharp transition from the classical case turns into a smooth crossover for the quantum case. The reason for that is that the destructive interference is destroyed for interacting particles in the quantum case. However, we showed that the crossover sharpens back to a classical transition by using a pseudoclassical method upon increasing the number of particles, or decreasing the effective Planck constant \hbar .

Acknowledgements. We thank A. Andreanov for useful discussions. This work was supported by the Institute for Basic Science, Project Code (Project No. IBS-R024-D1). PSM acknowledges financial support of the Ministry of High Education and Science of the Russian Federation through grant FSRZ-2023-0006.

-
- [1] E. J. Bergholtz and Z. Liu, Topological flat band models and fractional chern insulators, *Int. J. Mod. Phys. B* **27**, 1330017 (2013).
 [2] O. Derzhko, J. Richter, and M. Maksymenko, Strongly

- correlated flat-band systems: The route from heisenberg spins to hubbard electrons, *Int. J. Mod. Phys. B* **29**, 1530007 (2015).
 [3] D. Leykam, A. Andreanov, and S. Flach, Artificial flat

- band systems: from lattice models to experiments, *Advances in Physics: X* **3**, 1473052 (2018).
- [4] D. Leykam and S. Flach, Perspective: Photonic flat-bands, *APL Photonics* **3**, 070901 (2018).
- [5] J. Vidal, R. Mosseri, and B. Douçot, Aharonov-bohm cages in two-dimensional structures, *Phys. Rev. Lett.* **81**, 5888 (1998).
- [6] J. Vidal, B. Douçot, R. Mosseri, and P. Butaud, Interaction induced delocalization for two particles in a periodic potential, *Phys. Rev. Lett.* **85**, 3906 (2000).
- [7] M. Tovmasyan, E. P. van Nieuwenburg, and S. D. Huber, Geometry-induced pair condensation, *Phys. Rev. B* **88**, 220510 (2013).
- [8] M. Tovmasyan, S. Peotta, L. Liang, P. Törmä, and S. D. Huber, Preformed pairs in flat Bloch bands, *Phys. Rev. B* **98**, 134513 (2018).
- [9] Y. Kuno, T. Orito, and I. Ichinose, Flat-band many-body localization and ergodicity breaking in the Creutz ladder, *New J. Phys.* **22**, 013032 (2020).
- [10] Y. Kuno, T. Mizoguchi, and Y. Hatsugai, Interaction-induced doublons and embedded topological subspace in a complete flat-band system, *Phys. Rev. A* **102**, 063325 (2020).
- [11] C. Danieli, A. Andreanov, and S. Flach, Many-body flat-band localization, *Phys. Rev. B* **102**, 041116 (2020).
- [12] C. Danieli, A. Andreanov, T. Mithun, and S. Flach, Nonlinear caging in all-bands-flat lattices, *Phys. Rev. B* **104**, 085131 (2021).
- [13] C. Danieli, A. Andreanov, T. Mithun, and S. Flach, Quantum caging in interacting many-body all-bands-flat lattices, *Phys. Rev. B* **104**, 085132 (2021).
- [14] I. Vakulchyk, C. Danieli, A. Andreanov, and S. Flach, Heat percolation in many-body flat-band localizing systems, *Phys. Rev. B* **104**, 144207 (2021).
- [15] T. Orito, Y. Kuno, and I. Ichinose, Nonthermalized dynamics of flat-band many-body localization, *Phys. Rev. B* **103**, L060301 (2021).
- [16] T. Čadež, Y. Kim, A. Andreanov, and S. Flach, Metal-insulator transition in infinitesimally weakly disordered flat bands, *Phys. Rev. B* **104**, L180201 (2021).
- [17] Y. Kim, T. Čadež, A. Andreanov, and S. Flach, Flat band induced metal-insulator transitions for weak magnetic flux and spin-orbit disorder, arXiv preprint arXiv:2211.09410 (2022).
- [18] S. Lee, A. Andreanov, and S. Flach, Critical-to-insulator transitions and fractality edges in perturbed flat bands, *Physical Review B* **107**, 014204 (2023).
- [19] P. S. Muraev and A. R. Kolovsky, Quantum transport in a one-dimensional flux rhombic lattice, *Quantum Electronics* **51**, 502 (2021).
- [20] C. Danieli, A. Maluckov, and S. Flach, Compact discrete breathers on flat-band networks, *Low Temperature Physics* **44**, 678 (2018), <https://doi.org/10.1063/1.5041434>.
- [21] M. Fitzpatrick, N. M. Sundaresan, A. C. Li, J. Koch, and A. A. Houck, Observation of a Dissipative Phase Transition in a One-Dimensional Circuit QED Lattice, *Physical Review X* **7**, 011016 (2017).
- [22] G. Fedorov, S. Remizov, D. Shapiro, W. Pogosov, E. Egorova, I. Tsitsilin, M. Andronik, A. Dobronosova, I. Rodionov, O. Astafiev, and A. Ustinov, Photon transport in a Bose-Hubbard chain of superconducting artificial atoms, *Physical Review Letters* **126**, 180503 (2021).
- [23] J. G. C. Martinez, C. S. Chiu, B. M. Smitham, and A. A. Houck, Interaction-induced escape from an Aharonov-Bohm cage [10.48550/arXiv.2303.02170](https://arxiv.org/abs/10.48550/arXiv.2303.02170) (2023).
- [24] A. Szameit, D. Blömer, J. Burghoff, T. Schreiber, T. Pertsch, S. Nolte, A. Tünnermann, and F. Lederer, Discrete nonlinear localization in femtosecond laser written waveguides in fused silica, *Optics Express* **13**, 10552 (2005).
- [25] G. Cáceres-Aravena, D. Guzmán-Silva, I. Salinas, and R. A. Vicencio, Controlled Transport Based on Multiorbital Aharonov-Bohm Photonic Caging, *Physical Review Letters* **128**, 256602 (2022).
- [26] Notice, that from the viewpoint of a laboratory experiment the classical limit $\hbar \rightarrow 0$ corresponds to scaling the nonlinearity of the oscillator energy spectrum as $U = \hbar g$, and the driving strength as $\Omega \rightarrow \Omega/\sqrt{\hbar}$.
- [27] G. Kordas, D. Witthaut, P. Buonsante, A. Vezzani, R. Burioni, A. Karanikas, and S. Wimberger, The dissipative bose-hubbard model: Methods and examples, *The European Physical Journal Special Topics* **224**, 2127 (2015).
- [28] Attractors of this type were discussed earlier in Refs. [32, 33] with respect to exciton-polariton dynamics in two coupled micro-cavities. If we associate the A and B sites of our system with these two cavities then, by driving the C -site, we pump the antibonding mode of the $A - B$ system but it is the bonding mode which is subject to decay.
- [29] This follows from the fact that for $g = 0$ the single-particle density matrix of N identical particles coincides with the density matrix of a single particle.
- [30] A. A. Bychek, D. N. Maksimov, and A. R. Kolovsky, Decay of symmetry-protected quantum states, *Physical Review A* **102**, 033324 (2020).
- [31] A. R. Kolovsky, Quantum coherence, evolution of the Wigner function, and transition from quantum to classical dynamics for a chaotic system, *Chaos: An Interdisciplinary Journal of Nonlinear Science* **6**, 534 (1996).
- [32] K. Rayanov, B. Altshuler, Y. Rubo, and S. Flach, Frequency Combs with Weakly Lasing Exciton-Polariton Condensates, *Physical Review Letters* **114**, 193901 (2015).
- [33] C. Lledó and M. H. Szymańska, A dissipative time crystal with or without Z_2 symmetry breaking, *New Journal of Physics* **22**, 075002 (2020).